metals

MDPI

Article

Effects of Lubricating Conditions on Wear Performance of U77MnCrH Rail

Xu Liang [1], Xikai Wei [2], Yingqi Li [1], Meng Wang [1] and Fengshou Liu [1,*]

[1] Metals and Chemistry Research Institute, China Academy of Railway Sciences, Beijing 100081, China; liangxu@rails.cn (X.L.); lee_jh@rails.cn (Y.L.); wm_93934@rails.cn (M.W.)
[2] Postgraduate Department, China Academy of Railway Sciences, Beijing 100081, China; jinfeng@rails.cn
* Correspondence: liufengshou@rails.cn; Tel.: +86-186-1218-3254

Abstract: With the rapid development of railway towards being high speed and having heavy load capacity, the wheel–rail wear and rolling contact fatigue in the curve section with a small radius of freight have become the key problems in urban railways, which need to be solved urgently. The aims of this study were to compare the wear resistance with three different lubricating conditions on wheel–rail wear based on the wheel–rail rolling contact simulation tests. The wear loss, microhardness, and microstructure of the contacted surface of the rail were detected systematically. The results showed that the wear rates of rail were reduced by 71% for grease lubrication and 55% for solid lubrication, compared to those without lubrication. At the same time, the thickness of plastic deformation layer of rail samples were about 167 μm for the dry state, 138 μm for the solid lubrication state, and 128 μm for the oil lubrication state, respectively. It indicates that the thickness of the plastic deformation layer was significantly reduced under both grease and/or solid lubricating conditions. In addition, the microstructure of the deformation layer with two kinds of lubricated states was coarser and denser than that without lubricants. The average grain size of the deformation layer was approximately 0.22 μm under dry conditions and 0.32 μm under lubricated conditions. It also indicated that the changes in lubricants did not have a significant effect on the average grain size of the deformation layer. The results of the present study could provide theoretical reference for the development and design of lubricants used as rail materials.

Keywords: rails; friction and wear; lubricant; microhardness; microstructure

Citation: Liang, X.; Wei, X.; Li, Y.; Wang, M.; Liu, F. Effects of Lubricating Conditions on Wear Performance of U77MnCrH Rail. *Metals* **2024**, *14*, 414. https://doi.org/10.3390/met14040414

Academic Editors: Badis Haddag and Slobodan Mitrovic

Received: 21 January 2024
Revised: 19 March 2024
Accepted: 26 March 2024
Published: 30 March 2024

1. Introduction

With the rapid development of rail transport, the speeds of trains are gradually increasing, which have put forward the higher requirements for the safety and stability of railway systems [1–3]. The daily operation and maintenance of the wheel–rail are also facing new technical challenges, especially for the heavy haul railways and urban rail systems with small curve radii. There are mainly two reasons for these challenges. First, railway wheels operate in a demanding environment with high normal contact forces and significant tangential forces. The resulting stresses often exceed the yield stress of the as-manufactured wheel material, leading to plastic flow, wear, and fatigue damage [4]. The other reason is that the curved steel rails with small radii have always been the top priority in railway track maintenance and repair [5]. The lateral force of the small-radius curved wheels and rails is relatively large, and the rails suffer from varying damages such as side wear, wave wear, and rolling contact fatigue, which seriously restrict and affect the service life and safety of the small-radius curved rails. It also leads to the increase in costs and the decrease in service life of wheels and rails [6–8]. Moreover, surface damage and friction have become the important problems for affecting the running safety and passenger comfort. It is known that wheel–rail contact is often an open system contact that is influenced by various environmental conditions, such as temperature, humidity, water,

and even leaves [9]. All these environmental factors affect the friction and wear between wheel and rail. To remain competitive with other forms of transport, it is necessary to keep the costs and capital investments minimum in the railway industry. In recent years, although the friction modification technology and the lubricant products used between wheels and rails have been widely developed and applied [10], a more effective friction modification technology or lubricant product is still urgently necessary to achieve lower friction losses. Therefore, the correct use and selection of lubricants has become a vital issue to improve the wear properties of rails, particularly of small-radius curved rails.

Regarding this issue, lubricants between wheels and rails have been widely investigated. It is well known that rail lubrication can reduce the friction coefficient of the contact interface between the wheel and the rail to about 0.1, thus alleviating the rail wear and fatigue damage. It is an effective method to maintain good wear properties during service even in the small-radius curved rails [11–14]. Commonly, the friction modification between the wheel and the rail could be divided into two kinds, i.e., rail side lubrication and top-of-rail (TOR) friction modification. The problems of rail side wear and noise could be easily solved by the addition of lubricants, but it is different from the TOR friction modification. TOR friction modifiers entail the direct application of lubricating material (TOR friction modifiers) onto the top surface of the steel rail. In order to maintain the safety of a train during its operation, TOR friction modifiers should have a "moderate friction coefficient level", i.e., the friction (adhesion) coefficient of the wheel tread/rail head interface should be controlled within the range of 0.1–0.3 [15]. In other words, TOR friction correction technology not only reduces friction to decrease wear loss but also meets the adhesion coefficient requirements for normal traction and braking of trains. Therefore, the selection and use of lubricants on the TOR is an important anti-friction technique for extending the service life of rails and reducing the costs of railways during operation and maintenance.

Presently, there are various types of lubricant materials, including oil-based, water-based, oil-like, and solid-like, with varying lubrication effects [16]. Oil-like and solid-like lubricants are the most common lubricating materials to be used in rails to simultaneously reduce wear loss and improve wear performance. However, most studies were focused on the formation and propagation mechanism of rolling contact fatigue cracks between wheels and rails. And the results showed that the water and oil often lead to low adhesion during contact, and it accelerates the propagation of pre-existing cracks because of the fluid hydrostatic pressure. With the significant improvement in rail performance, the formation of cracks becomes less likely to occur, and the wear resistance of high-performance rails before cracks still needs attention, but the effect of different lubricant materials on the wear of novel high-performance rails (U77MnCrH) is rarely reported. In addition, previous references were mostly focused on qualitative reports on the wear mechanism with or without lubrication conditions. The present study would quantitatively investigate the wear weight loss, the thickness, and the microstructure evolution of the plastic deformation layer during wear under different lubrication conditions. This study aims to increase the knowledge about the lubrication of contacted interface of high-performance rails, more specifically, about the effect of lubrication materials on the wear of high-performance rails.

In the present study, the wear loss, microhardness, and microstructure of the contacted surface of the high-performance rail with three different lubricating conditions were investigated based on the wheel–rail rolling contact simulation tests. It could provide theoretical reference for the development and design of lubricants used in high-carbon high-performance rails.

2. Materials and Methods

A GPM-30A rolling contact fatigue testing machine was used during friction and wear experiments under dry and various lubrication conditions, which could load a vertical load of 1.2~30 kN and the rotation rate could be smoothly regulated between 5 and 2000 r/min. The standard of GB/T 10622-1989 was applied to test and machine samples. By setting the rotation speed of the main and assistant shafts, the slip ratio could meet the experimental

requirements. The diagram of the testing machine and the sample is shown in Figure 1. Three replicas of each wear condition were used to improve the testing results, and the average was reported in this paper.

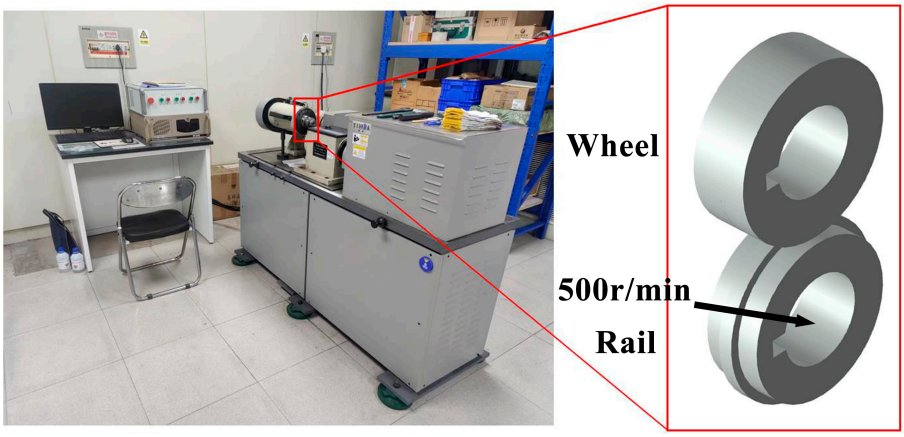

Figure 1. Schematic diagram of the contact mode between the test equipment and rail samples.

The rail material was named as U77MnCrH, and the wheel material was CL65. Tables 1 and 2 provide the chemical composition and the corresponding mechanical properties, respectively. Based on their chemical composition, it is obvious that wheel steel was a hypoeutectoid steel, while rail steel was an eutectoid steel. The contents of Mn and Cr in rail steel were higher than those in CL65 steel, while the contents of Mo and V were lower than those in CL65 steel. In addition, it is observed that the tensile strength, yield strength, elongation, reduction in area, and hardness of the rail at room temperature were 1262 MPa, 718 MPa, 13.25%, 40%, and 371 HBW, respectively, while they were 1077 MPa, 697 MPa, 15.50%, 41%, and 333 HBW, respectively, for CL65 steel. It demonstrated that the strength and the hardness of CL65 steel were significantly lower than that of U77MnCrH, but the elongation and reduction in area of the rail were only slightly higher that those of the wheel. In addition, Figure 2a,b give the microstructures obtained by the optical microscope (OM) of rail and wheel, and their corresponding scanning electron microscopes (SEM) microstructures are shown in Figures 2c and 2d, respectively. It indicated that the microstructure of the rail mainly consisted of pearlite, while the microstructure of the wheel comprised pearlite and ferrite, and the ferrite was distributed along grain boundaries. The volume fractions of the ferrite and pearlite was calculated to be 9.8% and 90.2% by the Image Pro Plus software. Moreover, a software of Nano Measurer was applied to determine the pearlite interlamellar spacing of the rail and wheel from the corresponding SEM images. The statistical results shows that the pearlite interlamellar spacing of the rail is 196 ± 12.4 μm, while it is 311 ± 23.6 μm for the wheel. The soft phase of ferrite and the larger pearlite interlamellar spacing lead to the decrease of strength and hardness in wheel, compared to that in rail. The microstructure was shown to be consistent with the mechanical properties.

Table 1. The chemical composition of rail and wheel materials (wt.%).

Steels	C	Mn	Si	Ni	Cr	Cu	Mo	V
U77MnCrH	0.786	0.958	0.450	0.076	0.370	0.099	0.0006	--
CL65	0.632	0.781	0.651	0.010	0.090	0.010	0.002	0.020

Table 2. Mechanical properties of rail and wheel materials.

Steels	Tensile Strength (MPa)	Yield Strength (MPa)	Elongation (%)	Reduction in Area (%)	Surface Hardness (HBW)
U77MnCrH	1262	718	13.25	40	371
CL65	1077	697	15.50	41	333

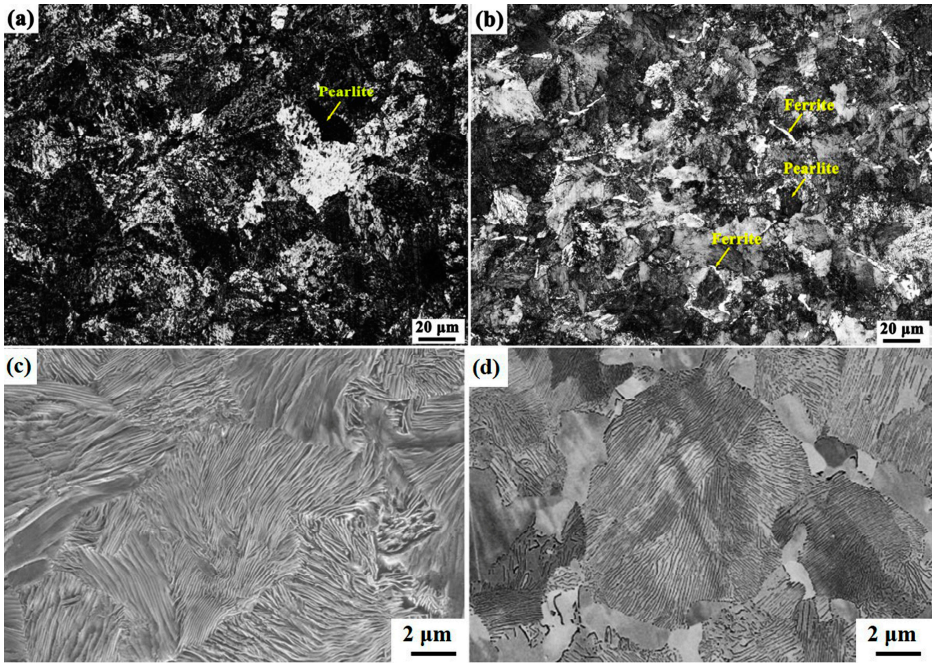

Figure 2. OM microstrcuture (**a**,**b**) and SEM microstrcuture (**c**,**d**) of the matrix: (**a**,**c**) rail and (**b**,**d**) wheel.

Based on the relevant references of some heavy-duty lines, the experimental stress of 1200 MPa was applied, and the following experimental conditions were selected according to Hertzian contact theory [17,18]. The vertical load was 1400 N, and the outer edge curvature of the steel rail sample was 200 mm, and the width of the boss was 5 mm. Table 3 provides the specific experimental parameters. It should be noted that a slip of 0.5–2% is usually assumed during the laboratory rolling contact experiments. However, in this study, due to the research location being the side wear position, the proportion of sliding friction is greater than that of the tread position, so the slip of 4% is assumed. Similarly, a high contact stress of 1200 MPa is selected for the experiment. This is because the simulated wear test conditions of this experiment mainly involve the wear at the contact points between the wheels and the upper steel rail when a 30t axle load train passes through an 800 m radius curve. Due to the small contact spot between the wheel and the rail, the contact stress sharply increases, and the contact stress at the side wear position could reach 1200~1800 MPa. Moreover, the shape and size of the test samples are shown in Figure 3. It is known that the outer edge of the wheel sample was flat.

Table 3. Experimental parameters.

Rail	Contact Stress	Interface Status	Vertical Force	Wheel	Slip	Number of Revolutions	Speed of Main Shaft
U77MnCrH	1200 MPa	Dry Grease Solid	1400 N	CL65	4%	50,000	500 r/min

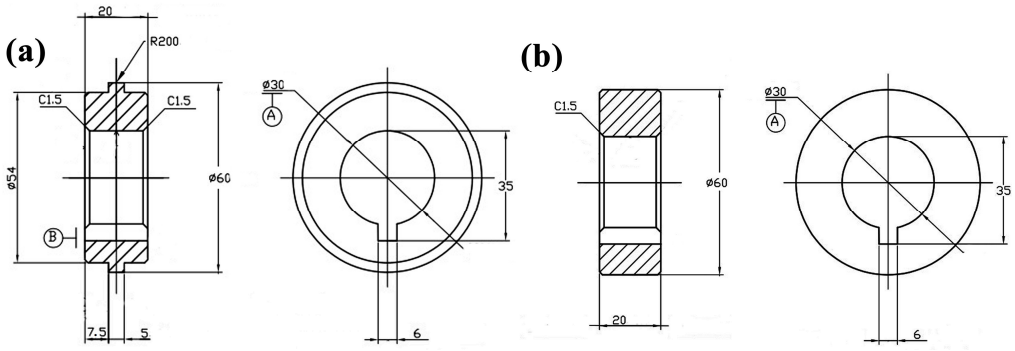

Figure 3. Schematic diagram of samples: (**a**) rail and (**b**) wheel.

During the wear tests at room temperature, the grease lubricant was dripped using a needle tube, while the solid lubricant was applied by hands. The density, kinematic viscosity, water content, and pour point of grease lubricant produced by Tianjin Qihong Fine Chemical Co., Ltd., Tianjin, China, were 0.9 g/cm^3, 135 mm^2/s, 0%, and −40 °C, respectively. It was composed of a crosslinker, basis grease, and an anti-wear agent. The crosslinker had C9 and C5 petroleum resin, polyethylene wax of grades 100 and 120, masterbatch, terpene resin, aldehyde ketone resin, and paraffin wax of grades 100, 108, and 140. In addition, the basis grease consisted of lithium stearate base grease of grades Nos. 1, 2, and 3, as well as calcium sulfonate base grease of grades Nos. 1, 2, and 3. The anti-wear agent was composed of graphite, molybdenum disulfide, copper powder, melamine (MCA), polytetrafluoroethylene (PTFE), and zinc powder. In contrast, the solid lubricant with the superior environmental performance was provided by Beijing China Railway Science and Technology Co., Ltd., and its model was TK SL-V. Its hardness was 40 A according to the standard of GB/T 2411. Moreover, its ingredients included the thickener of polyurea, base oil of mineral oil, and cagasin (HVI650 and PAO), and additives such as T361A, melamine (MCA), zinc salt of butyl octyl thiophosphate (ZDDP), T561, and diphenylamine.

Figure 4 shows the schematic diagram of adding lubricants. The adding frequency was determined by the dynamic friction coefficient at the contact position of the sample. When the number of revolutions reached 5000, the lubricant was added for the first time, and the friction coefficient after adding the lubricant should not be less than 0.1 [19,20]. The next cycle of adding lubricants began when the dynamic friction coefficient reached above 0.5. The additional amount used each time was 20 µL for the grease lubricant and 20 mg for the solid lubricant, respectively [21]. It is noted that the adding frequency/volume applied in wear testing was obtained according to the theoretical calculation and the measurable dynamic friction coefficient [21].

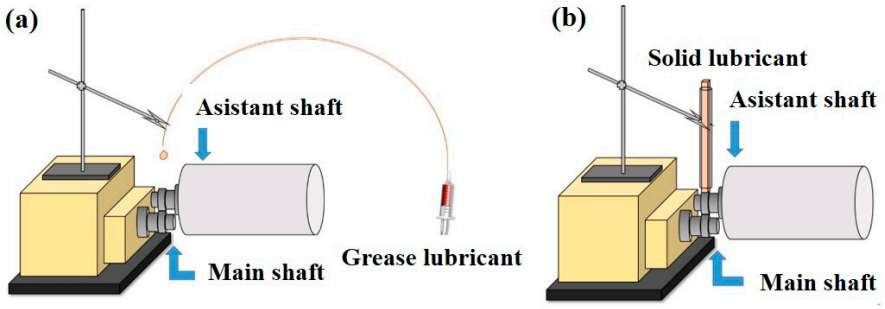

Figure 4. Schematic diagram of adding lubricants: (**a**) grease lubricant and (**b**) solid lubricant.

The hardness of the contact surface of all samples after wear test was determined by a Vickers hardness tester with a load of 0.10 kgf and a loading time of 10 s. The microstructure after wear tests was observed by a Zeiss optical microscope and a Nano 400 field emission scanning electron microscope (FE-SEM). The samples under various lubrication conditions were cut along the rotation direction (longitudinal), and they were embedded, polished,

and etched in 4% nital before observation. In addition, the distribution of grain sizes was revealed by electron backscatter diffraction (EBSD) with a scanning step of 0.15 μm at a voltage of 20 kV with an Oxford operating system. The hardness was detected by the Vickers hardness tester. It is noted that the hardness within the top 50 microns of the sample was detected by the Hysitron TI980 nanoindentation tester due to the limitation in experimental condition.

3. Results and Discussion

3.1. Wear Loss

Figure 5a gives the friction coefficient curves between the rail and wheel during the whole wear test under different lubrication conditions. In addition, after 50,000 rotations wear tests, the wear losses of U77MnCrH and CL65 under dry, grease, and solid lubrication conditions are compared and the results are shown in Figure 5b. It is obvious that under the current lubricating conditions, the wear loss under grease lubrication is less than that under solid lubrication, indicating that the wear reduction effect of grease lubricant is better than that of solid lubricant. Compared with the wear loss under dry lubrication conditions, it reveals that both grease and solid lubricants play an important role in lubricating and lowering wear loss. The wear loss ratio (lubrication/dry condition) of the grease lubricant is about 71%, while it is about 55% for the solid lubricant. It could be attributed to the fact that the oil film thickness under the grease lubricating condition is thicker than that under the solid lubricating condition, and the shear strength under the grease lubricating condition is greater [22,23], resulting in the lowest wear loss. In addition, the largest total wear loss is detected in the dry samples. It is because the wear performance of the rail is related to surface hardening and the wear coefficient under the dry condition increases sharply [24,25].

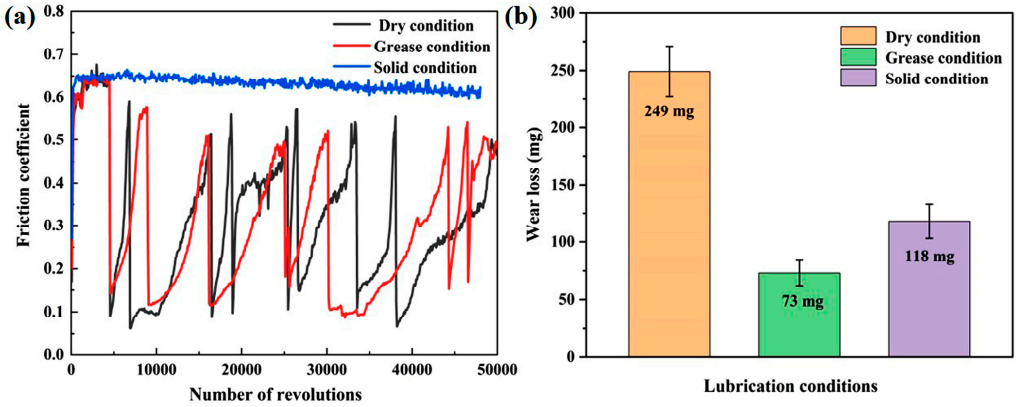

Figure 5. (**a**) Friction coefficient curves and (**b**) wear loss of rail samples under different lubrication conditions.

3.2. Hardness

The change trends of hardness on the transverse sections from the contact surface hardening layer to the matrix under different lubrication conditions are shown in Figure 6. The hardness of the sample decreases with the increase in the distance between the contacted surface and the matrix and finally stabilizes between 350 and 400 HV under all lubrication conditions. The various hardness values are related to the distribution of the microstructure. It can be seen from Figure 6 that the hardness of the sample under dry conditions enters a stable floating stage at a distance of about 250 μm, while this stage is reached at about 150~200 μm under the grease and solid lubrication conditions. When the suffered yield stress of the contacted material exceeds its yield strength during the rolling contact process of the wheel and the rail, the wheel and the rail will undergo plastic deformation and form a hardening layer. After a sufficient rolling contact, the thickness of the plastic deformation layer eventually is stabilized at the exact value. The results given

in Figure 6 indicate that the addition of lubricants effectively lowers the thickness of the surface hardening layer.

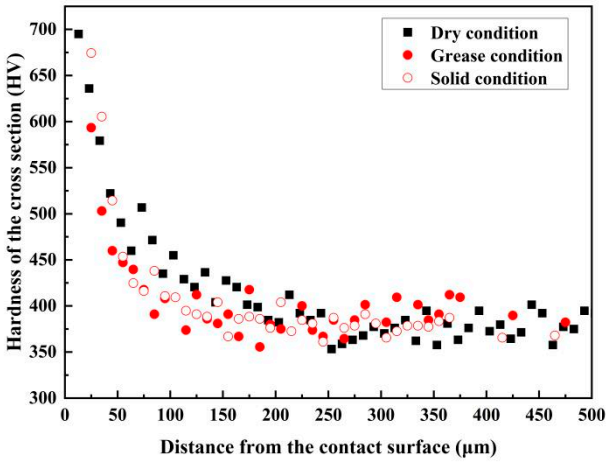

Figure 6. Hardness gradient on the cross-section of rails under different lubrication conditions.

In addition, in order to accurately analyze the change trend of hardness in the deformation layer and to avoid the limitation of Vickers hardness tester, the Hysitron TI980 nanoindentation tester is used to determine the evolution of hardness within the top 50 μm of the deformation layer. The measuring points are designed as two rows of points that diverge from each other at a distance of about 15 μm. The first point is about 5 μm away from the contacted surface. The interval between the two points in the same row is about 5 μm. The pressure of the indenter is set to be 10,000 μN. The loading time, holding time, and unloading time are 5, 2, and 5 s, respectively. The position of the points is shown in Figure 7, and the left side of the view field is the contacted surface of the rail materials.

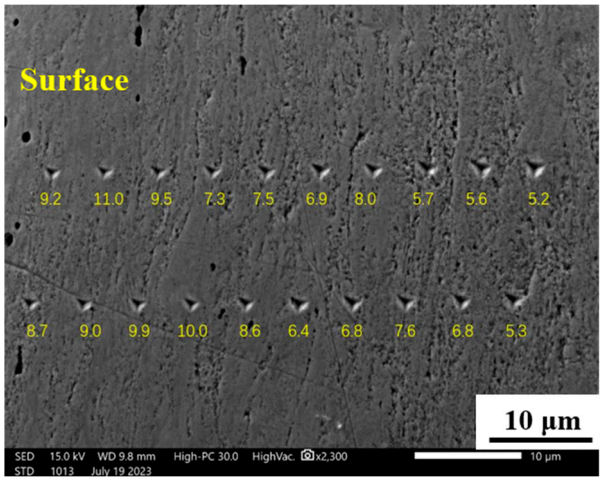

Figure 7. Nanoindentation on the surface deformation layer of rails under grease lubrication condition.

Based on the above measurements, the hardness gradient within a depth of 50 μm initiated at the contact surface is obtained. In addition, according to Appendix F of Standard ISO 14577-1-2015, an empirical conversion relationship between indentation hardness, H_{IT}, and hardness, HV, is obtained. Indentation hardness, H_{IT} (MPa), and Vickers hardness, HV (kgf/mm^2), could be transferred equivalently by the following Equations (1) and (2):

$$H_{IT} = \frac{F}{A_P} \quad (1)$$

$$HV = \frac{1}{g_n} \times \frac{F}{A_S} \quad (2)$$

where g_n is the gravitational acceleration of 9.80665 m/s^2; A_p is the projected area of the indenter; and A_s is the surface area of the indentation.

Therefore, it can be seen that the Vickers hardness in HV could be obtained by the corresponding hardness in H_{IT} with a conversion factor. For any depth of indentation, the ratio of the projected area (A_p) of the indenter to the surface area (A_s) of the indentation is a constant. In the present study, an improved glass-type indenter with an angle of 65.27° between the surface of the pyramid indenter and the axial direction is used. According to the results reported in reference [26], it is known that the ratio of A_p/A_s is 0.9083. Therefore, Equation (3) can be obtained as follows.

$$HV = 10^3 \times \frac{1}{g_n} \times \frac{A_P}{A_S} \times \frac{F}{A_P} = 10^3 \times \frac{1}{g_n} \times \frac{A_P}{A_S} \times H_{IT} = 92.62H_{IT} \quad (3)$$

Figure 8 shows the nanoindentation test results of U77MnCrH within a depth of 50 μm in the plastic deformation layer initiated at the contact surface under different lubrication conditions. It indicates that the hardness decreases with the increase in the depth of the deformation layer. As mentioned above, the plastic deformation will be formed on the surface of the sample during the wear process. The contacted surface has the highest hardness value due to the most severe deformation. In addition, the hardness values under dry, solid lubricant, and grease lubricant conditions increase sequentially. It implies that the surface work hardening effect under grease lubrication is the most obvious after a certain wear time before cracks, leading to the lowest total wear loss. It is consistent with the wear loss result shown in Figure 5. The main reason is that, after adding grease lubricant, the grease material will easily adhere to the surface of the sample, and the deformation on the surface of the wear sample will increase cyclically without diffusing deeper into the matrix. It leads to the densest deformation microstructure. In addition, under the dry condition, in the surface deformation layer, the process of dynamic recovery and recrystallization is easier to occur due to the highest friction temperature and deformation stress [27–29]. Therefore, the hardness value under the dry condition is lowest on the top 50 μm deformation layer, while it is highest under the grease lubrication condition. And it is known that a lower hardness of wear materials will result in a higher wear loss. The lowest hardness value is observed under the dry condition when compared with those under grease and solid lubricating conditions, leading to the largest wear loss of wear samples under the dry condition. It is also consistent with the results shown in Figure 5.

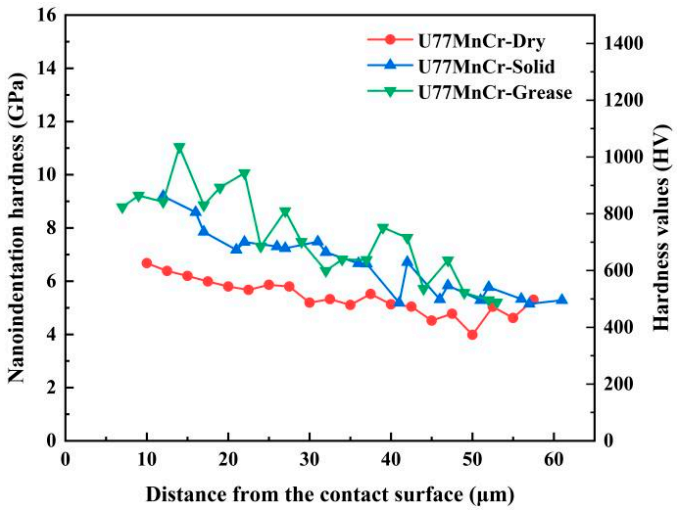

Figure 8. Nanoindentation test results of U77MnCrH under different lubricating conditions.

3.3. Microstructure

Figure 9 provides the OM microstructure of the obvious plastic deformation layer of the dry, solid lubrication, and grease lubrication samples, respectively. It is obvious that the lesser the distance from the contacted surface, the more robust the microstructure. In addition, the thickness of the plastic deformation layer could be measured by their corresponding OM images, and it is about 167 µm for the dry state, 138 µm for the solid lubrication state, and 128 µm for the oil lubrication state, respectively. It indicates that the plastic deformation layer of the contact surface of the rail is deepest under the dry condition, which is consistent with the analysis results of the hardness gradient in Figure 6. Under the grease and/or solid lubrication conditions, the thickness of the plastic deformation layer of the rail is thinner than that under the dry condition. It could be caused by the higher fraction coefficient. Under the dry condition, the fraction coefficient is obviously higher that that under the lubrication condition, leading to the larger pressure on the surface. Therefore, the deepest deformation layer is obtained under the dry condition.

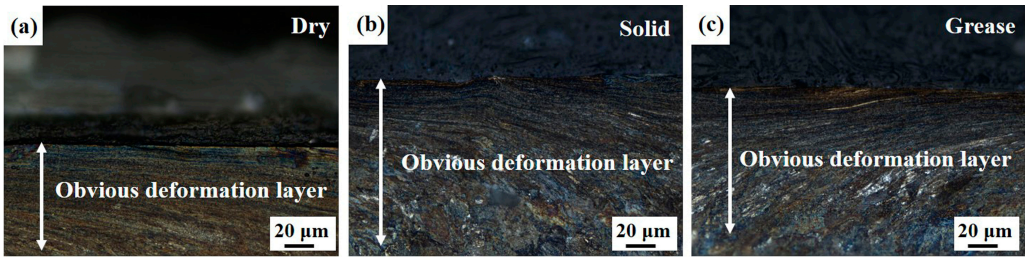

Figure 9. OM microstructure of the obvious plastic deformation layer of different sample cross-sections: (**a**) under dry condition; (**b**) under solid lubricant condition; and (**c**) under grease lubricant condition.

Figure 10 shows the IPF images of the EBSD analysis, showing the distribution of grain size of the surface deformation layer under different lubrication conditions. The number and size of grains in the field of view are provided in Table 4. It can be seen from Figure 10 that the grain size on the top surface is the finest, and it increases with the depth of the plastic deformation layer until it is equal to the grain size of the matrix. Therefore, as the depth in the plastic deformation layer increases, the hardness gradually decreases until it reaches the matrix level. In addition, compared with the grease/solid lubricating conditions, the smallest grain size is obtained in the samples subjected to the dry condition. In this case, under dry friction conditions, the work of plastic deformation increases, thereby promoting a better grain refinement. At the same time, heating increases and hardness decreases due to the relaxation of internal stresses. In this case, the grain size can remain very small. If a lubricant is used, the intensity of deformation is simply reduced due to less friction. And this also leads to a decrease in temperature in the tribocontact zone and, therefore, less pronounced stress relaxation due to surface heating. The result is slightly larger grains than with dry friction, but higher hardness due to lower stress relaxation. Here, it is noted that although the finer microstructure causes higher hardness due to the fine grain strengthening effect [30,31], the hardness is also significantly related to the dislocation density in deformation samples [32,33]. Under the dry condition, the occurrence of dynamic recovery and recrystallization leads to the lowest dislocation density, and thus, the hardness value in the 50 µm plastic deformation layer is smallest even with the smallest grain sizes.

Table 4. Number and average grain size of grains in the surface deformation layer.

Lubrication Condition	Number of Grains	Average Grain Size (µm)
Dry	7196 ± 27	0.22 ± 0.03
Solid	3650 ± 31	0.32 ± 0.04
Grease	3770 ± 16	0.33 ± 0.02

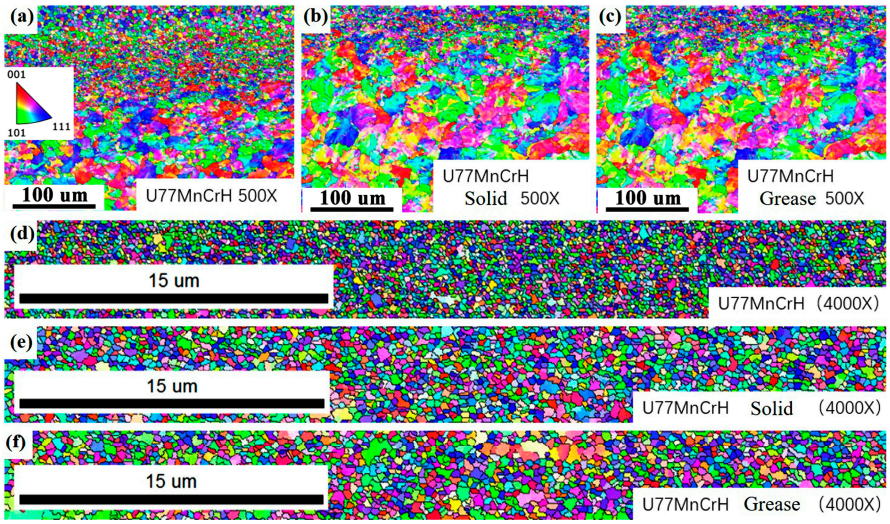

Figure 10. EBSD analysis of wear samples on cross-section under different lubrication conditions with different magnification: (**a**) 500× and (**d**) 4000× under dry condition; (**b**) 500× and (**e**) 4000× under solid lubricant condition; and (**c**) 500× and (**f**) 4000× under grease lubricant condition.

Figure 11 shows the SEM microstructure of the wear surface of the rail samples under different lubrication conditions. It manifests that, under the same wear test conditions, the microstructure of samples with lubricating medium is denser than that of the dry sample. This could be related to the formation of the protection oil film due to the addition of lubricants. The formation of the protection film leads to a lower wear loss. In addition, there are no obvious cracks found on the contacted interfaces of all three samples. It implies that the rail of U77MnCrH has a superior matching of strength and toughness. Apart from this reason, it also could be related to the contact stress and the wear time during the present wear test. The grease and solid lubricants quickly dried up and formed a solid lubricant layer after being applied to the wheel–rail contact interface. In addition, there is an interesting intrinsic reason for the similar microstructures produced during wear under grease and solid lubrication conditions. It may be related to the number of wear cycles and the chemical composition of lubricants. The different effect mechanisms of different lubricants on cracks and fatigue will be further discussed in detail in the future.

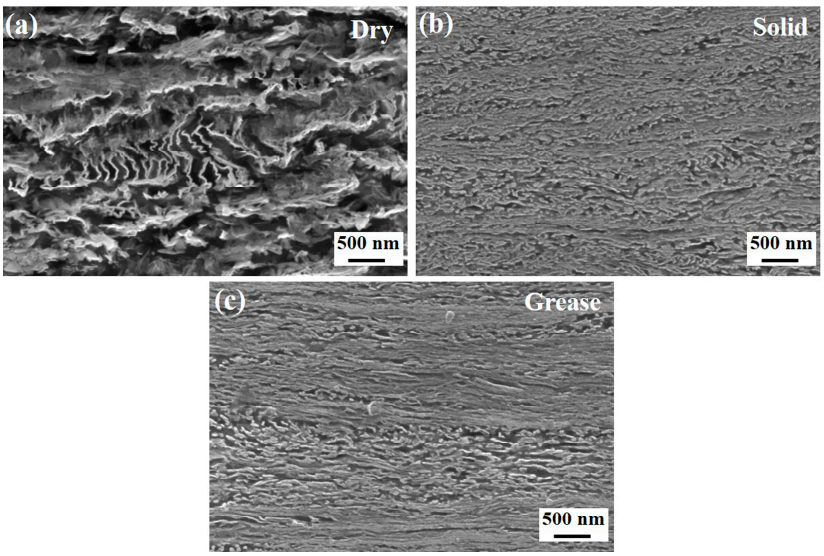

Figure 11. SEM microstructure of the contacted surface under (**a**) dry condition; (**b**) solid lubricant condition; and (**c**) grease lubricant condition.

The main novelty of the present study is the wear weight loss, the thickness, and microstructure evolution of the plastic deformation layer during the wear process under different lubrication conditions between the CL65 steel and the high-performance rail steel (U77MnCrH). The results showed that the thickness and the microstructure of the plastic deformation layer are rarely affected by the type of lubricants. In other words, the types of lubrication materials, i.e., grease and solid lubricants, selected by the present study had little effect on the thickness and the microstructure of the deformation layer, when the high-performance rails, i.e., U77MnCrH, were tested.

4. Conclusions

In this study, the effects of different lubricating materials on the wear performance of the high-performance U77MnCrH were investigated based on the wheel–rail rolling contact simulation tests. The main conclusions that can be drawn are as follows:

(1) Both grease and solid lubricants played an important role in reducing wear loss. Under the current experimental conditions, the rates of wear loss of U77MnCrH were reduced by 71% for grease lubrication and 55% for solid lubrication, compared with that under the dry condition.
(2) The thickness of plastic deformation layer of rail was measured to be 167 μm for the dry state, 138 μm for the solid lubrication state, and 128 μm for the oil lubrication state, respectively. The thickness of the plastic deformation layer was largest under dry lubricating conditions.
(3) The microstructure of the deformation layer was coarser and denser under the two lubricated states compared to that under the dry condition. The lubricants types had little effect on average grain sizes.

Author Contributions: Conceptualization, F.L. and X.L.; Methodology, X.L.; Software, Y.L.; Validation, F.L., X.L. and M.W.; Formal analysis, X.W.; Investigation, X.L.; Resources, X.L.; Data curation, M.W.; Writing—Original Draft Preparation, X.L. and X.W.; Writing—Review and Editing, F.L. and Y.L.; Visualization, X.L.; Supervision, F.L.; Project Administration, F.L.; Funding acquisition, F.L. All authors have read and agreed to the published version of the manuscript.

Funding: The authors gratefully acknowledge the financial supports from National Key Research and Development Program of China (No. 2021YFB2601000), the Development Project of China Railway (No. N2022G011), and China Academy of Railway Sciences Corporation Limited within the Major Issues of the Fund (No. 2023YJ052).

Data Availability Statement: The raw data supporting the conclusions of this article will be made available by the authors on request.

Conflicts of Interest: The authors declare that this study received funding from China Academy of Railway Sciences Corporation Limited. The funder was not involved in the study design, collection, analysis, interpretation of data, the writing of this article or the decision to submit it for publication.

References

1. Cao, Y.; An, Y.T.; Su, S.; Guo, X.; Sun, Y.K. A statistical study of railway safety in China and Japan 1990–2020. *Accid. Anal. Prev.* **2022**, *175*, 106674. [CrossRef]
2. Zhang, S.Y.; Spiryagin, M.; Lin, Q.; Ding, H.H.; Wu, Q.; Guo, J.; Liu, Q.Y.; Wang, W.J. Study on wear and rolling contact fatigue behaviors of defective rail under different slip ratio and contact stress conditions. *Tribol. Int.* **2020**, *169*, 107491. [CrossRef]
3. Zhang, S.Y.; Spiryagin, M.; Ding, H.H.; Wu, Q.; Guo, J.; Liu, Q.Y.; Wang, W.J. Rail rolling contact fatigue formation and evolution with surface defects. *Int. J. Fatigue* **2020**, *158*, 106762. [CrossRef]
4. Hu, Y.; Watson, M.; Maiorino, M.; Zhou, L.; Wang, W.J.; Ding, H.H.; Lewis, R.; Meli, E.; Rindi, A.; Liu, Q.Y.; et al. Experimental study on wear properties of wheel and rail materials with different hardness values. *Wear* **2021**, *477*, 203831. [CrossRef]
5. Wang, Z.Q.; Lei, Z.Y. Analysis of influence factors of rail corrugation in small radius curve track. *Mater. Sci.* **2021**, *12*, 31–40. [CrossRef]
6. Zhu, Y.; Wang, W.J.; Lewis, R.; Yan, W.Y.; Lewis, S.R.; Ding, H.H. A review on wear between railway wheels and rails under environmental conditions. *J. Tribol.* **2019**, *141*, 120801. [CrossRef]

7. Ding, H.H.; Mu, X.P.; Zhu, Y.; Yang, W.B.; Xiao, Q.; Wang, W.J.; Liu, Q.Y.; Guo, J.; Zhou, Z.G. Effect of laser claddings of Fe-based alloy powder with different concentrations of WS2 on the mechanical and tribological properties of railway wheel. *Wear* **2022**, *488–489*, 204174. [CrossRef]
8. Kvarda, D.; Skurka, S.; Galas, R.; Omasta, M.; Shi, L.B.; Ding, H.H.; Wang, W.J.; Krupka, I.; Hartl, M. The effect of top of rail lubricant composition on adhesion and rheological behaviour. *Eng. Sci. Technol.* **2022**, *35*, 101100. [CrossRef]
9. Shebani, A.; Iwnicki, S. Prediction of wheel and rail wear under different contact conditions using artificial neural networks. *Wear* **2018**, *406–407*, 173–184. [CrossRef]
10. Tomeoka, M.; Kabe, N.; Tanimoto, M.; Miyauchi, E.; Nakata, M. Friction control between wheel and rail by means of on-board lubrication. *Wear* **2022**, *253*, 124–129. [CrossRef]
11. Allmaier, H. Increase service life for rail wheel bearings—A review of grease lubrication for this application. *Lubricants* **2022**, *10*, 36. [CrossRef]
12. Kvarda, D.; Galas, R.; Omasta, M.; Shi, L.B.; Ding, H.H.; Wang, W.J.; Krupka, I.; Hartl, M. Asperity-based model for prediction of traction in water-contaminated wheel-rail contact. *Tribol. Int.* **2021**, *157*, 106900. [CrossRef]
13. Stock, R.; Stanlake, L.; Hardwick, C.; Yu, M.; Eadie, D.; Lewis, R. Material concepts for top of rail friction management-classification, characterization and application. *Wear* **2016**, *366–367*, 225–232. [CrossRef]
14. Aldajah, S.; Ajayi, O.O.; Fenske, G.R.; Kumar, S. Investigation of top of rail lubrication and laser glazing for improved railroad energy efficiency. *J. Tribol.* **2003**, *125*, 643–648. [CrossRef]
15. Zhao, X.J.; Chen, Q.; Liu, Y.S.; Qiu, X.Y.; Meli, E.; Rindi, A. Effects of slip ratio and contact stress on rolling contact fatigue of defected rail materials. *Eng. Fail. Anal.* **2022**, *131*, 105817. [CrossRef]
16. Żuchowski, R.; Nowoświat, A.; Kucharski, I. Reduction of tram noise by using a rail lubrication device. *Appl. Acoust.* **2023**, *210*, 109429. [CrossRef]
17. Knothe, K. History of wheel/rail contact mechanics: From Redtenbacher to Kalker. *Veh. Syst. Dyn.* **2008**, *46*, 9–26. [CrossRef]
18. Lewis, R.; Magel, E.; Wang, W.J.; Olofsson, U.; Lewis, S.; Slatter, T.; Beagles, A. Towards a standard approach for the wear testing of wheel and rail materials. *Proc. Inst. Mech. Eng. Part F J. Rail Rapid Transit* **2017**, *231*, 760–774. [CrossRef]
19. Li, Q.; Wu, B.N.; Ding, H.H.; Galas, R.; Kvarda, D.; Liu, Q.Y.; Zhou, Z.R.; Omasta, M.; Wang, W.J. Numerical prediction on the effect of friction modifiers on adhesion behaviours in the wheel-rail starved EHL contact. *Tribol. Int.* **2022**, *170*, 107519. [CrossRef]
20. Galas, R.; Kvarda, D.; Omasta, M.; Krupka, I.; Hartl, M. The role of constituents contained in water-based friction modifiers for top-of-rail application. *Tribol. Int.* **2017**, *117*, 87–97. [CrossRef]
21. Messaadi, M.; Oomen, M.; Kumar, A. Friction modifiers effects on tribological behaviour of bainitic rail steels. *Tribol. Int.* **2019**, *140*, 105857. [CrossRef]
22. Li, J.X.; Wu, B.N.; Ding, H.H.; Galas, R.; Omasta, M.; Wen, Z.F.; Guo, J.; Wang, W.J. Wear and damage behaviours of wheel and rail materials: Effects of friction modifier and environmental temperature. *Wear* **2023**, *523*, 204796. [CrossRef]
23. Biazon, L.; Ferrer, B.P.; Toro, A.; Cousseau, T. Correlations between rail grease formulation and friction, wear and RCF of a wheel/rail tribological pair. *Tribol. Int.* **2021**, *153*, 106566. [CrossRef]
24. Huang, Y.B.; Shi, L.B.; Zhao, X.J.; Cai, Z.B.; Liu, Q.Y.; Wang, W.J. On the formation and damage mechanism of rolling contact fatigue surface cracks of wheel/rail under the dry condition. *Wear* **2018**, *400–401*, 62–73. [CrossRef]
25. Molyneux-Berry, P.; Davis, C.; Bevan, A. The influence of wheel/rail contact conditions on the microstructure and hardness of railway wheels. *Sci. World J.* **2014**, *2014*, 209752. [CrossRef] [PubMed]
26. Kim, W.; Lee, K.; Kim, J.-H.; Kim, Y.-C.; Kwon, D. A further study on knoop indentation plastic deformation for evaluating residual stress. *Korean J. Met. Mater.* **2020**, *58*, 515–521. [CrossRef]
27. Li, N.; Kingkam, W.; Han, R.H.; Tang, M.; Zhang, H.X.; Zhao, C.Z. Effect of dynamic recrystallization on the transformed ferrite microstructures in HSLA steel. *Metals* **2020**, *10*, 817. [CrossRef]
28. Elwazri, A.M.; Wanjara, P.; Yue, S. Dynamic recrystallization of austenite in microalloyed high carbon steels. *Mater. Sci. Eng. A* **2019**, *339*, 209–215. [CrossRef]
29. Cottrell, A. Dynamical recovery. *J. Mater. Sci.* **2004**, *39*, 3865–3870. [CrossRef]
30. Tian, J.Y.; Wang, H.X.; Zhu, M.; Zhou, M.X.; Zhang, Q.; Su, X.; Guo, A.M.; Xu, G. Improving mechanical properties in high-carbon pearlitic steels by replacing partial V with Nb. *Mater. Sci. Eng. A* **2022**, *834*, 142622. [CrossRef]
31. Tian, J.Y.; Xu, G.; Hu, H.J.; Wang, X.; Zurob, H. Transformation kinetics of carbide-free bainitic steels during isothermal holding above and below MS. *J. Mater. Res. Technol.* **2020**, *9*, 13594–13606. [CrossRef]
32. Zhang, X.D.; Hansen, N.; Gao, Y.K.; Huang, X.X. Hall-Petch and dislocation strengthening in graded nanostructured steel. *Acta Mater.* **2012**, *60*, 5933–5943. [CrossRef]
33. Uchima, H.; Kumagai, M.; Shimbe, J.; Tanabe, A.; Mizuno, Y.; Onuki, Y. Impact of dislocation density and mobility on yielding behavior in quenched medium-carbon martensitic steel tempered at low temperature. *ISIJ Int.* **2022**, *62*, 998–1003. [CrossRef]